AIP Journal of Applied Physics

Connectivity and critical current density of in-situ processed MgB2 superconductors: Effect of excess Mg and non-carbon based additives

P. P. S. Bhadauria, Anurag Gupta, Hari Kishan, and A. V. Narlikar

Citation: Journal of Applied Physics **115**, 183905 (2014); doi: 10.1063/1.4875664
View online: http://dx.doi.org/10.1063/1.4875664
View Table of Contents: http://scitation.aip.org/content/aip/journal/jap/115/18?ver=pdfcov
Published by the AIP Publishing

Connectivity and critical current density of *in-situ* processed MgB_2 superconductors: Effect of excess Mg and non-carbon based additives

P. P. S. Bhadauria,[1] Anurag Gupta,[1,a)] Hari Kishan,[1] and A. V. Narlikar[2]
[1]*National Physical Laboratory (CSIR), Dr. K. S. Krishnan Road, New Delhi 110012, India*
[2]*UGC-DAE Consortium for Scientific Research, University Campus, Khandwa Road, Indore 452017, MP, India*

(Received 3 April 2014; accepted 28 April 2014; published online 13 May 2014)

In a sequel to our previous paper (J. Appl. Phys. **113**, 036908 (2013)), where we reported comprehensive analysis of inter-grain connectivity (A_F), pinning, percolation threshold (P_c), and anisotropy (γ) in a series of *ex-situ* processed MgB_2, we address the same issues in *in-situ* processed samples. MgB_2 samples with stoichiometric composition, excess Mg (5 wt. %) and further 3 wt. % addition of various non-carbon based additives like nano-Ag, nano-Ni, and YBCO are synthesised by the *in-situ* route. Detailed investigations of X-ray diffraction, magnetization (M), and resistivity (ρ) as a function of temperature (T) and field (B) in the range 5–300 K and 0–8 T are carried out in all the samples. The resistive superconducting onset $T_{con} \sim 38.6 \pm 0.3$ K and offset (where ρ goes to zero) $T_{c0} \sim 38.1 \pm 0.3$ K of the samples stay nearly unchanged. The inter-grain connectivity (A_F) of the samples varies between 11%–20%. All the additives result in a critical current density (J_c) higher than the stoichiometric MgB_2 sample, where the highest values (e.g., $J_c(1\,T, 5\,K) \sim 1.2 \times 10^9$ A/m^2) are observed for the sample with 5 wt. % excess Mg. The major findings based on quantitative analysis of ρ (T, B) and J_c (B, T) data in all the samples are: (1) along with previously studied *ex-situ* samples, the $J_c(A_F)$ shows a significant increase at $A_F \sim 7\%$; (2) the irreversibility lines lie lower than the characteristic $T_{c0}(B)$ lines in the B-T phase diagram; (3) a universal core pinning (δl- and/or δT_c- type) mechanism is revealed in the entire T range 5–30 K; and (4) typical values of $P_c \sim 0.57 \pm 0.04$ is indicative of weak link networks. © *2014 AIP Publishing LLC*. [http://dx.doi.org/10.1063/1.4875664]

I. INTRODUCTION

After the discovery of superconductivity in MgB_2,[1] improvement of J_c under magnetic field via processing[2–9] and flux pinning[10–15] has been a very active research area. Despite the effort, MgB_2 continues to pose challenges linked with inter-grain connectivity, pinning, and anisotropy. Both carbon and non-carbon based additives have been tried extensively in improving the $J_c(B)$. Having fewer fabrication parameters, for application purpose, the *ex-situ* synthesis route has been used by several researchers.[5–7,16] Since the substitution reactions and trapping of nano-particles to create effective pins can easily occur via *in-situ* route, it has been a favourite for nano-additives. Carbon, on substituting into lattice, drives MgB_2 to dirty limit to enhance B_{c2},[14–18] which is supposed to be the key reason of high field J_c increase. In comparison, the non-carbon based additives like Mg, Ag, Ni, Fe, Al, YBCO, etc.[19–29] have met with only a limited success. A relevant question that needs attention in the latter case, before detailed J_c optimization is undertaken, is whether the non-carbon additives truly work as pinning centres or they merely influence the connectivity of the samples. In the present work, we investigate the structural, transport, and magnetic properties of *in-situ* processed pure MgB_2 and with various non-carbon based additives to quantitatively address this question. Detailed analysis based on Rowell's connectivity model,[30] collective pinning theory[31] and anisotropy based percolation model[32] is carried out to understand the $J_c(B,T)$ behaviour. In continuation to our previous report,[29] where samples with connectivity ranging from ~0.01% to 7% were addressed, the same is furthered up to ~20% by *in-situ* processing. The highlight of the present work is that processing and the choice of additive affect all these parameters that govern the overall $J_c(B, T)$ of the samples.

II. EXPERIMENTAL DETAILS

Polycrystalline bulk MgB_2 samples in pure form and with different non-carbon based additives, were prepared by *in-situ* solid state synthesis route. Powders of Mg (Riedel-de-Haen, purity 99%) and B (Fluka, purity 95%–97%) were mixed in appropriate ratios to prepare pure MgB_2, $MgB_2 + 5$ wt. % Mg and the latter composition with added 3 wt. % of nano-Ag, nano-Ni, and $YBa_2Cu_3O_{7-\delta}$ (YBCO) powders. The powders were hand ground and mixed with an agate mortar pestle for an hour. This was followed by pelletization in a parallelepiped shape under a pressure of 10 MPa. The pellets were placed in an iron tube with a pin hole and sintered in Argon atmosphere at 800 °C for an hour followed by furnace cooling to room temperature. The samples are named as follows: pristine as "MB" and with additives as "MBd" (where d can be Mg, Ag, Ni, and YB for representing the additive Mg, $Mg + Ag$, $Mg + Ni$, and $Mg + YBa_2Cu_3O_{7-\delta}$, respectively). The samples were

a)Author to whom correspondence should be addressed. Electronic mail: anurag@nplindia.org

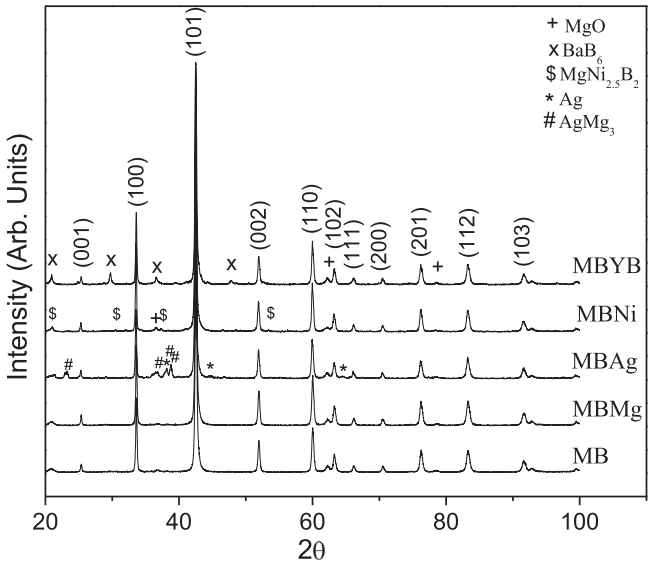

FIG. 1. The XRD patterns for various MgB_2 samples. The designated (hkl) peaks belong to the MgB_2 phase, while the impurity peaks are marked separately.

characterized by X-ray diffraction (XRD), and magnetization (M) and resistivity (ρ) in the temperature range 5–300 K and field range 0–8 T.

III. EXPERIMENTAL RESULTS

The XRD patterns of all the samples, as shown in Fig. 1, reveal MgB_2 as the dominant phase along with a presence of small amounts of additive dependent secondary phases. As often observed in bulk MgB_2, traces of MgO are found in all the samples.[33] In particular, the MBAg sample shows extra peaks at 38.1°, 44.1°, and 64.4° related to Ag, and 22.8°, 36.8°, 38.2°, and 38.8° related to $MgAg_3$ impurities.[23] In MBYB sample, the small peaks at 20.9°, 29.7°, 47.7°, and 36.5° mark the presence of BaB_6 impurity.[26] In MBNi sample, the impurity peaks at 20.9°, 30.6°, 37.3°, and 37.4° indicate the presence of $MgNi_{2.5}B_2$.[10] No significant shift is observed in the XRD peaks related with the main MgB_2 phase in any of the samples (see Fig. 1). The lattice parameters, calculated by FULLPROF program (based on Rietveld method) and listed in Table I, show no significant change by any of the additives.

The measured ρ(T) for all the samples, depicted in Fig. 2, show an expected normal state metallic behaviour and a sharp superconducting transition. Magnified view of the transition region showing $\rho(T)/\rho_{40}$ (where $\rho_{40} = \rho(40K)$) is

TABLE I. The values of lattice parameters "a" and "c" (Å), ρ_0 ($\mu\Omega$cm), A_F (%), RRR, T_{con} (K), T_{c0} (K), T_{cm} (K), and $J_c(10^8\,A/m^2)$ at 1 T and 5 K for various samples.

	a	c	ρ_0	RRR	A_F	J_c	T_{con}	T_{c0}	T_{cm}
MB	3.080	3.519	14.7	3.33	12.5	8.3	38.4	37.9	38.3
MBMg	3.080	3.519	14.9	3.42	11.9	12.4	38.9	38.2	38.2
MBAg	3.084	3.521	16.0	3.38	11.2	10.3	38.9	38.3	38.0
MBNi	3.083	3.522	10.1	3.10	20.3	9.7	38.7	37.8	37.5
MBYB	3.081	3.520	15.7	3.46	11.1	9.9	38.5	37.9	38.2

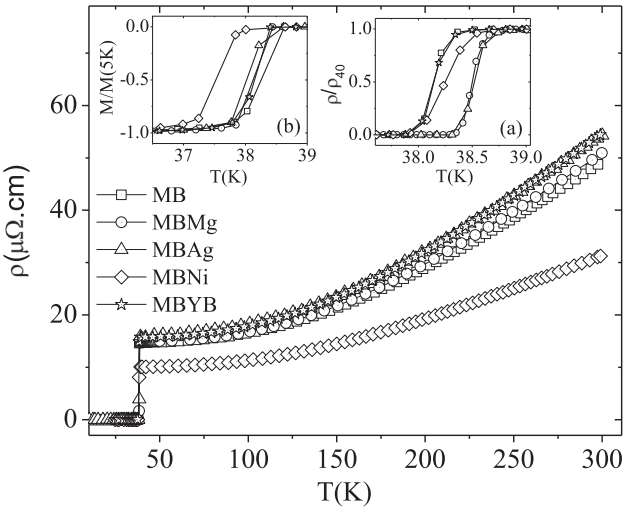

FIG. 2. Resistivity as a function of temperature for various MgB_2 samples. The insets show the magnified view of superconducting transitions: (a) transport and (b) magnetization.

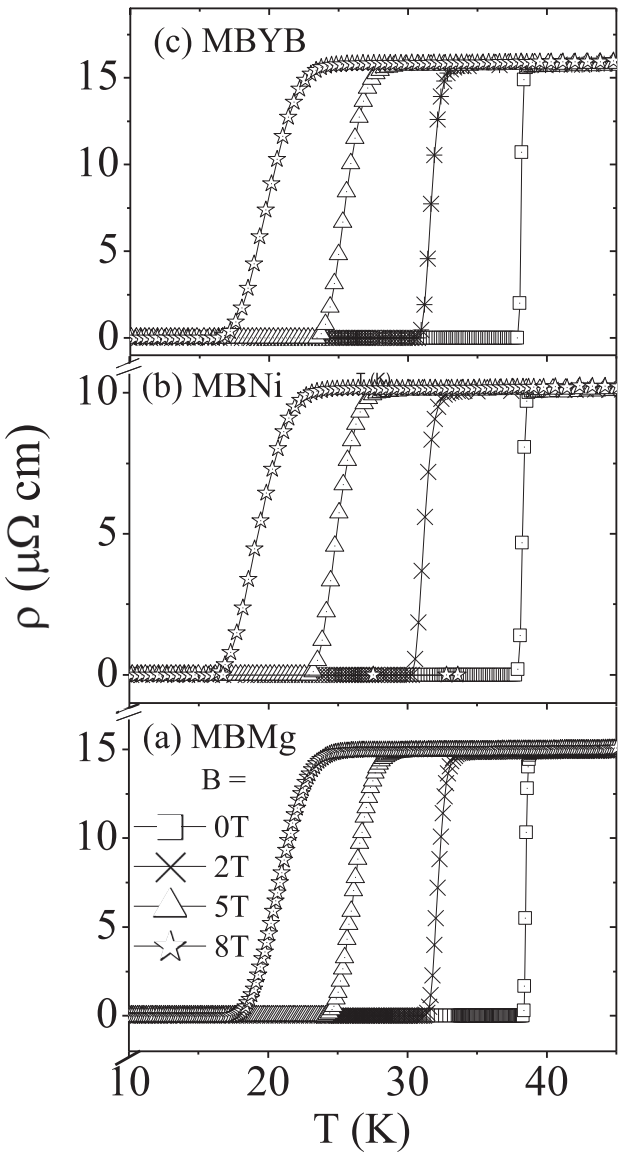

FIG. 3. Resistivity as a function of temperature at different applied magnetic fields for samples: (a) MBMg, (b) MBNi, and (c) MBYB.

plotted in inset (a) of Fig. 2. The values of ρ_{40}, the superconducting onset (T_{con}) and the zero resistivity temperature (T_{c0}) are shown in Table I. The sharpness of the superconducting transition and its bulk nature are confirmed by the M(T) measurements. For all the samples, the zero field cooled M(T)/M_5 (where $M_5 = M(5K)$) in an applied $B \sim 10$ mT is plotted in inset (b) of Fig. 2. The critical temperatures (T_{cm}, see Table I) corresponding to the midpoint of the diamagnetic transition match well with those obtained from the resistive transitions.

The ρ(T) of all the samples was measured in the presence of applied constant magnetic field. The same is shown for three samples MBMg, MBNi, and MBYB in Figs. 3(a)–3(c), respectively. In all the samples, with increasing B, the superconducting transition shifts to lower temperatures and the transition broadens. The change in T_{con} and T_{c0} as a function of B is plotted in Fig. 4 for all the samples. For comparison, the magnetically determined irreversibility field B*(T), discussed in next section, are also depicted in the same figure. In general, the characteristic T_{con}(B) line is steeper than T_{c0}(B) line, which is a reflection of broadening of the superconducting transition with increasing B.

The critical current density J_c(B) of all the samples was extracted, using Bean's model, from the isothermal M(B) hysteresis loops measured at various temperatures between 5 and 30 K. The J_c(B) at 5–30 K for all the samples are shown in Fig. 5. The samples with mixed non-carbon additives and/or excess Mg led to higher values of J_c(B, T) than pure MB sample. The MBMg sample having only excess Mg as additive showed the highest J_c at all the T and B. For comparison of J_c(5 K, 1 T) of different samples, see Table I.

IV. DISCUSSION

Besides pure MgB_2, samples having excess 5 wt. % Mg and additionally 3 wt. % of nano-Ag, nano-Ni, and YBCO prepared by the same *in-situ* route were studied. The lattice parameters of different samples do not show any significant

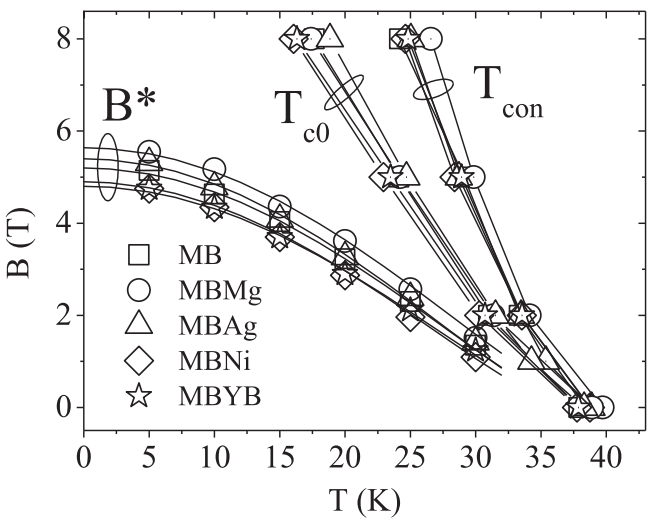

FIG. 4. The B-T phase diagram showing characteristic T_{con}(B), T_{c0}(B), and B*(T) for various MgB_2 samples. The solid lines through T_{con}(B) and T_{c0}(B) data are only a guide to eye, and B*(T) data are theoretical fits.

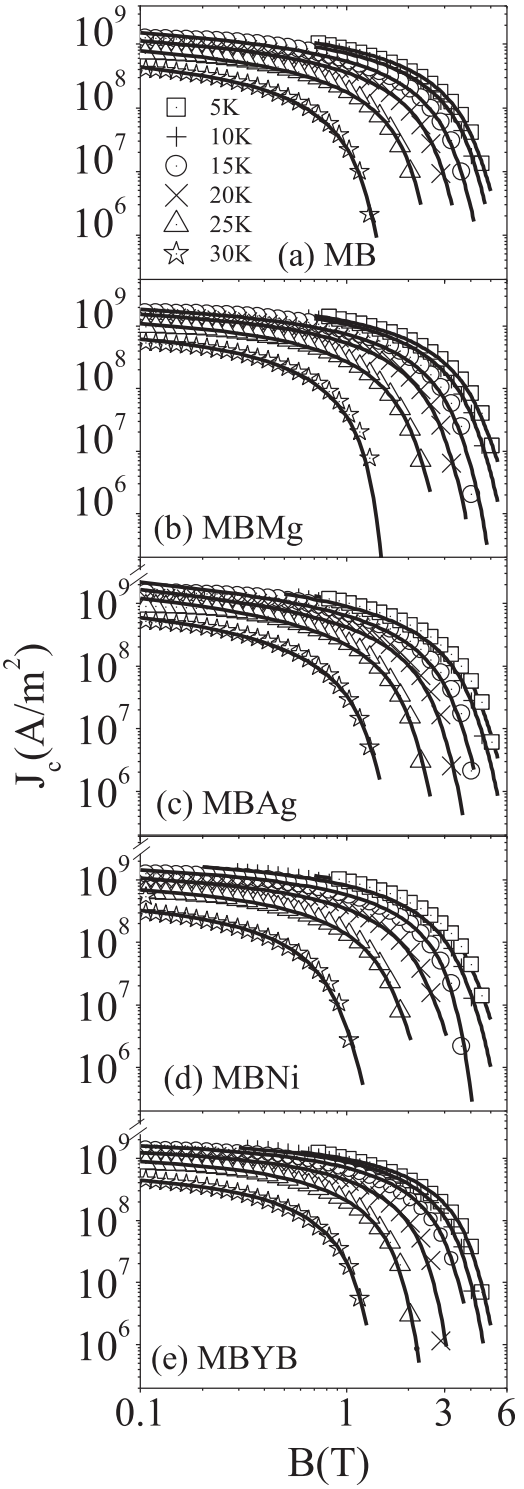

FIG. 5. Critical current densities as a function of applied magnetic field for various MgB_2 samples at T = 5 to 30 K. The solid lines represent theoretical fits.

change. This along with the fact that both T_{con} and T_{c0} do not change much reveals that none of the additives substitute in the lattice, which is in agreement with earlier reports.[21–24] One may conclude that the tried non-carbon additives apparently do not influence the intra-grain regions and may affect mainly the inter-grain regions of the samples. This should reflect in the normal state electrical transport. The resistivity of the samples is given by

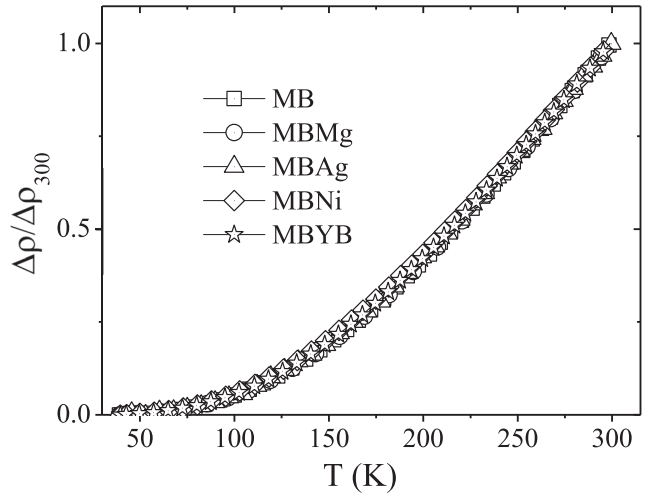

FIG. 6. Normalized $\Delta\rho$ as a function of temperature for various MgB_2 samples.

$$\rho(T) = \rho_0 + \Delta\rho(T), \tag{1}$$

where ρ_0 and $\Delta\rho$ are the T independent residual resistivity and T dependent part of the resistivity, respectively. Taking ρ_{40} as the respective ρ_0, for all the samples, we plot $\Delta\rho(T) / \Delta\rho_{300}$ in Fig. 6. The collapse of the data of all samples on a single curve shows that T dependence of the resistivity is identical in them. Along with the fact that there is no change in the intra-grain regions of the samples, the difference in the multiplicative factor of all the curves shown in Fig. 6 indicates the difference of the effective current carrying cross section area or connectivity (A_F) in various samples.[30] The A_F of the samples can be estimated by[30]

$$A_F = \Delta\rho_{300}(\text{single crystal})/\Delta\rho_{300}(\text{sample}), \tag{2}$$

where $\Delta\rho_{300}(\text{single crystal}) = 4.3\,\mu\Omega$ cm.[30] The values of A_F, ranging from 11%–20.3%, along with RRR and ρ_0 for all samples are listed in Table I. In comparison, the earlier reported *ex-situ* samples of MgB_2 prepared with different additives and sintering temperatures, had shown much smaller A_F values ~0.01% to 7%.[29] This shows that the *in-situ* processing leads to a significant increase of A_F.

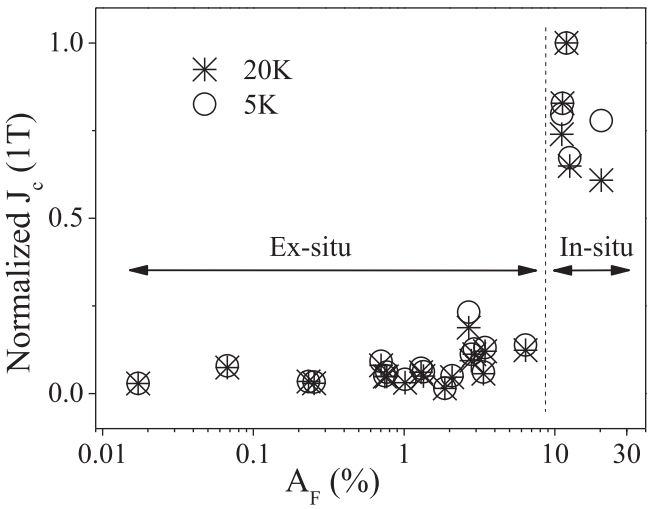

FIG. 7. Normalized values of J_c (1 T) at 5 K and 20 K as a function of connectivity (A_F) for various MgB_2 samples. The data in the region marked as *in-situ* is of the present samples and *ex-situ* is taken from references.[28,29]

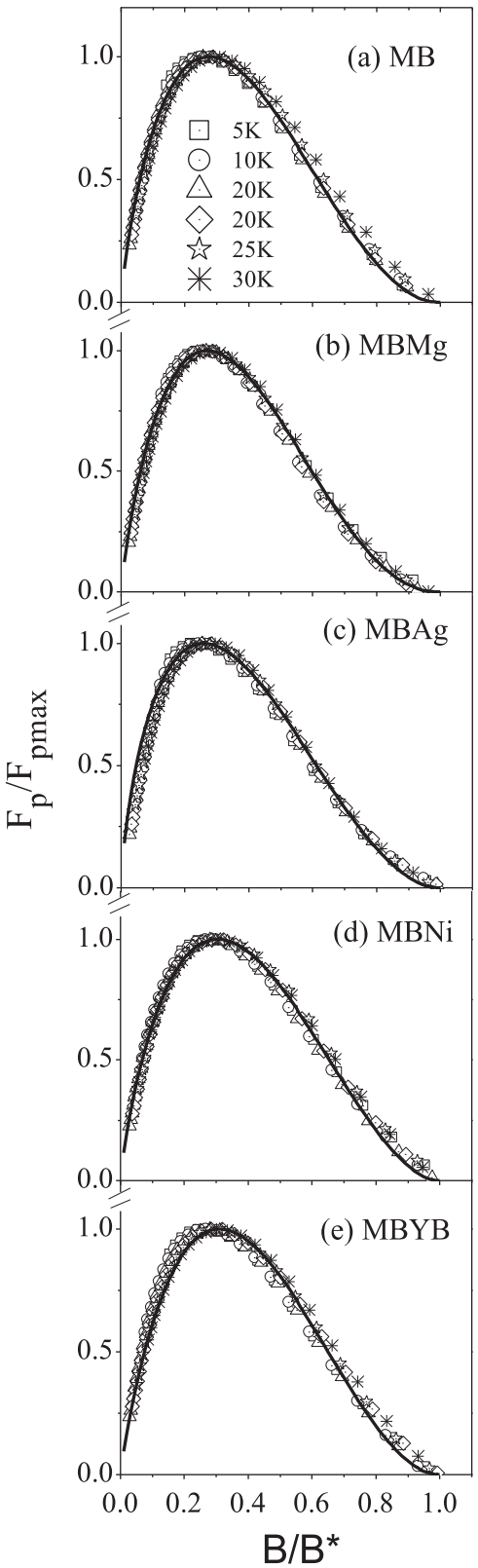

FIG. 8. Normalized pinning force density ($F_p/F_{p,max}$) as a function of reduced magnetic field (B/B*) for various MgB_2 samples at T = 5 to 30 K. The solid lines represent the theoretical fits.

TABLE II. $F_{p,\ max}(N/m^3)$, $B^*(T)$, p, q, b_{max}, and ratio $p/(p+q)$ at 5 K for various samples.

	$F_{p,\ max}$	B*	p	q	b_{max}	$p/(p+q)$
MB	8.56×10^8	5.15	0.80	2.1	0.28	0.28
MBMg	1.30×10^9	5.77	0.85	2.3	0.27	0.27
MBAg	1.04×10^9	5.32	0.70	2.0	0.26	0.26
MBNi	9.93×10^8	4.90	0.85	2.0	0.30	0.30
MBYB	1.01×10^9	4.88	0.90	2.0	0.31	0.31

We now discuss the impact of A_F on the J_c values. In the present *in-situ* samples, the J_c(5 K, 1 T) varies between 0.83–1.24 $\times$ 10^9 A/m^2 (see Table I), whereas the various *ex-situ* samples showed[29] nearly an order of magnitude smaller values 0.5–2.7 $\times$ 10^8 A/m^2. Following Rowell,[30] this result seems to be directly related with the fact that A_F values in the former samples are higher than in the latter. To see this quantitatively, in Fig. 7, we plot normalized values of J_c(5 K,1 T) and J_c(20 K,1 T) as a function A_F for all the samples measured in the present and earlier investigations.[28,29] The normalization has been carried out with the respective highest value of the J_c observed among all the samples. Many interesting features can be marked in Fig. 7. First, note that the $J_c(A_F)$ behaviour reflected by various samples is identical at both T = 5 and 20 K. Second, the J_c suddenly jumps to much higher values for A_F values higher than ~7%. It is tempting to conclude that 7% connectivity seems to be critical in terms of significant enhancement of J_c in bulk MgB_2. However, $A_F \sim 7\%$ also represents a boundary in Fig. 7, below (above) which all our *ex-situ* (*in-situ*) samples happen to lie. It would be interesting to cover the entire A_F range independently by both the methods and make a comparison. Third, no direct correlation between J_c and A_F is observed in either the *in-situ* or *ex-situ* samples. These features suggest that the material processing does set the low field J_c scale through the connectivity A_F of the sample. However, to understand the overall J_c(B,T) behaviour of all the samples, the influence of processing on other factors like pinning, upper critical fields (B_{c2}), weak link networks (WLN), and anisotropy needs to be analyzed, as was shown in the *ex-situ* case.[29]

For all the samples, J_c(B) sharply decreases towards zero at high fields (see Fig. 5). The field at which J_c(B) becomes typically smaller than ~10^6 A/m^2 is defined as a characteristic irreversibility field (B*) of the sample. We plot B* versus T for all the samples in Fig. 4, and the data are found to be described very well (see the fitted curves in Fig. 4) with the often used relation[11,12] $B^*(t) = B^*(0)(1\text{-}t^2)^{3/2}$, where $t = T/T_c$. The highest values of B*(T) are observed for MBMg sample. Note that the B*(T) curves of all the samples lie at a much lower position in comparison to the respective T_{c0}(B) and T_{con}(B) curves in the overall B-T phase diagram. This has been attributed to thermally activated depinning of the flux lines in bulk MgB_2.[34] For all the samples, the reduced pinning force density f (=F_p/F_{pmax}) as a function of reduced field b (=B/B*) at various temperatures is shown in Figs. 8(a)–8(e). In all the samples, perfect scaling of the f(b) curves observed at various T (=5–30 K) indicates same pinning mechanism operating at all $T < T_c$. The solid lines in Fig. 8 represent theoretical pinning curves given by $f \propto b^p(1\text{–}b)^q$, where the values of the exponents p and q, and b_{max} (where f(b) shows a maxima) depend upon the pinning mechanism.[35] The fact that, in case of all the samples, the ratio of $p/(p+q)$ match very well with the observed b_{max} (see Table II) establishes the goodness of the fitting.[35] For grain boundary (point core) pinning, the expected values of p = 0.5 (1), q = 2 (2), and b_{max} = 0.2 (0.33). In our samples (see Table II), the observed values of p = 0.7–0.9 and b_{max} = 0.26–0.31 indicate the presence of point core pinning mechanism. In addition, as shown in Fig. 9, the observed $F_{p,max} \propto B^{*2}$ dependence in all the samples supports the core pinning.[35] We would mention here that, in contrast, our previously[29] studied *ex-situ* samples showed p ~ 0.5, q ~ 2.0, and b = 0.15–0.23 reflecting mainly the grain boundary pinning.

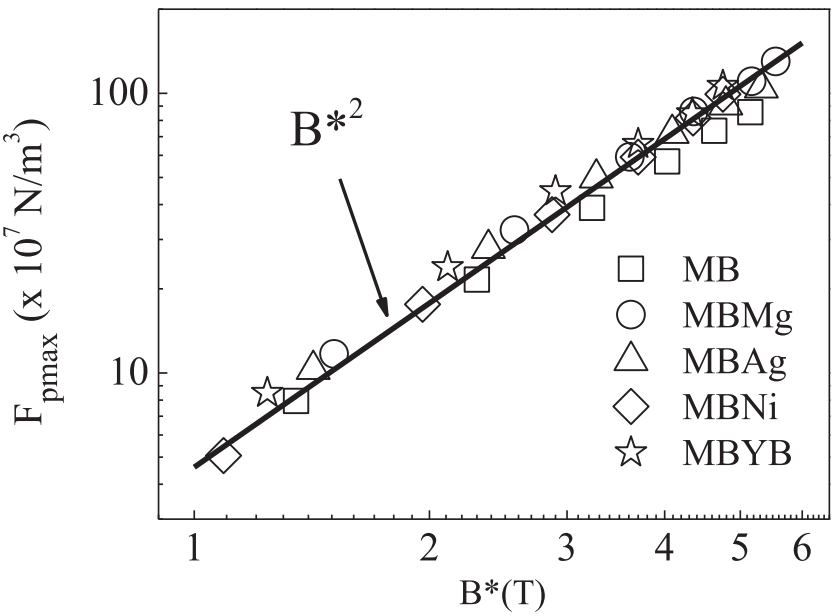

FIG. 9. Maximum pinning force density ($F_{p,max}$) as a function of irreversibility field (B^*) for various MgB_2 samples. The solid line shows that $F_{p,\ max}$ is proportional to B^{*2}.

According to the weak collective pinning theory,[31] with increasing B, the point core pinning should exhibit three regimes, namely: single-vortex, small-bundle (sb), and large-bundle. For $B < B_{sb}$, the inter-vortex interaction is negligible and each vortex in pinned independently. For $B > B_{sb}$, the inter-vortex interaction becomes important and vortices are collectively pinned in small bundles giving rise to $J_c(B)$ given by the relation[11,31]

$$J_c(B) \approx J_{c0}\exp\left[-\left(\frac{B}{B_0}\right)^n\right], \tag{3}$$

where J_{c0} and B_0 are constants and $n \sim 3/2$. Using Eq. (3) and plotting $\log[-\log(J_c(B)/J_{c0})]$ versus $\log(B)$, as done for MBMg in Fig. 10 at all T, the characteristic field B_{sb} is marked by departure of the data from a straight line at low field side. The values of $B_{sb}(T)$ so determined for all the samples are plotted in Fig. 11. The value of n showed a variation between 1.5 ± 0.3. For all the samples, the $B_{sb}(T)$ increases from 0.1 to 1.8 T with a decrease in T from 30–5 K that reflects an apparently similar behaviour. To understand the T dependence of B_{sb}, one needs to consider that the point core pinning can be caused either by spatial variation of T_c and/or mean free path leading to δT_c and/or δl type pinning, respectively. $B_{sb}(T)$ is given by[11,36]

$$\text{for } \delta T_c - \text{pinning} \quad B_{sb}(t) = B_{sb}(0)\left[\frac{1-t^2}{1+t^2}\right]^{2/3}, \tag{4}$$

$$\text{for } \delta l - \text{pinning} \quad B_{sb}(t) = B_{sb}(0)\left[\frac{1-t^2}{1+t^2}\right]^{2}. \tag{5}$$

The fits to the $B_{sb}(T)$ data using Eqs. (4) and (5) are depicted in Fig. 11. Interestingly, all the samples clearly reveal both δl- and δT_c- pinning, where the former (latter) is more dominant at lower (higher) T. In case of MB sample, the signature

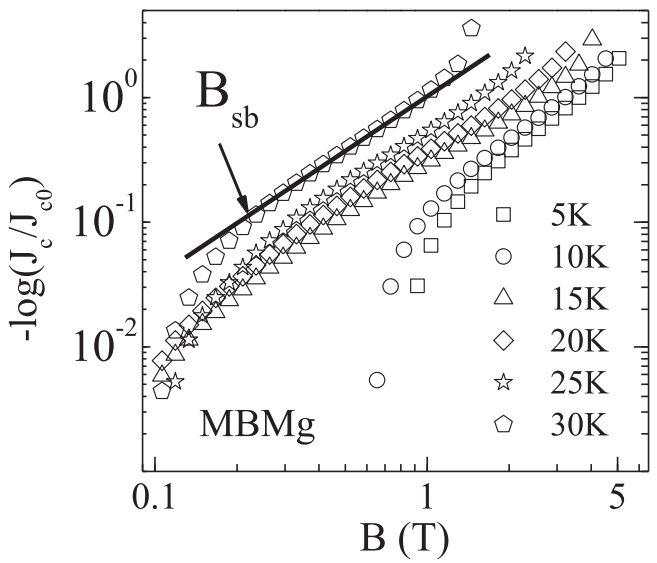

FIG. 10. The plot of $-\log[J_c/J_o]$ as a function of magnetic field for MBMg sample. B_{sb} marks the field at which the curves deviate from the straight line behaviour in the lower field region. As an example, this is illustrated for the 30 K data.

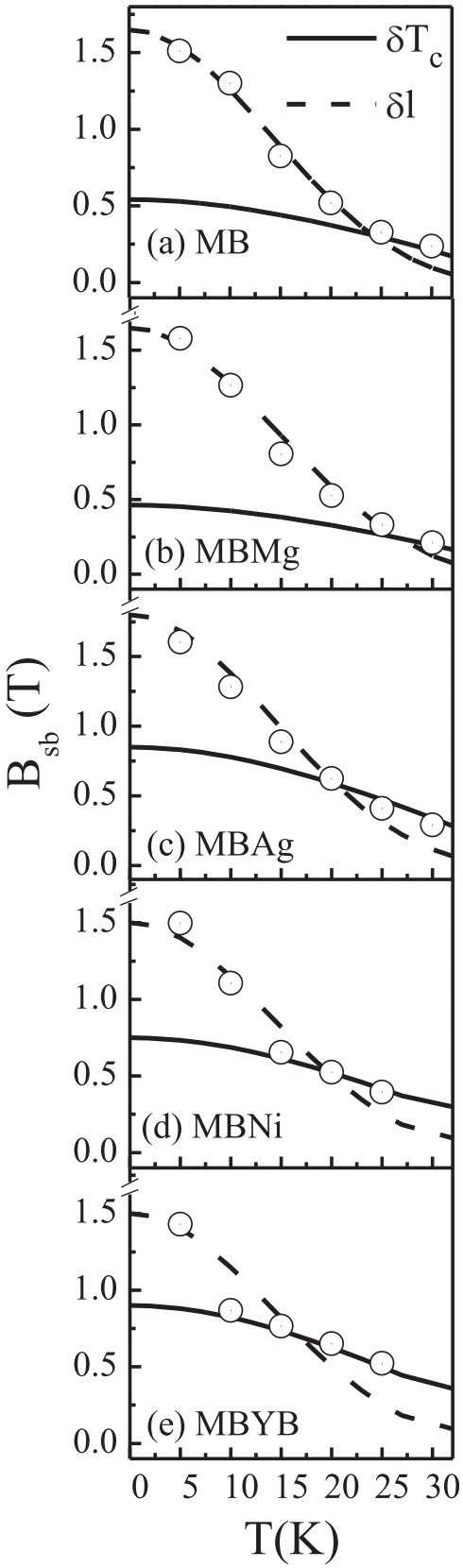

FIG. 11. B_{sb} as a function of temperature for various MgB_2 samples. The solid (dashed) lines represent theoretical fits to the δT_c (δl) pinning (see Eqs. (4) and (5)).

of δT_c- pinning is visible only at $T \sim 30$ K, which is further suppressed in the case of MBMg. Whereas, in case of the samples with various non-carbon additives, the δT_c-pinning

becomes pronounced at much lower T ~ 10–25 K. These results are compatible with the expected variation of local T_c across the sample, which should be highest in the case of mixed non-carbon elements.

The impact of other parameters like B_{c2}, γ, and WLNs on the overall $J_c(B, T)$ of different samples can be analyzed by applying Eisterer's anisotropy driven percolation model,[32] as reported earlier for our *ex-situ* samples.[29] In the present analysis, we use the experimentally observed pinning relation instead of the grain boundary pinning as originally assumed in the model.[32] The values of $B_{c2}^{\parallel}(T)$ (parallel to the ab-planes) are just the $T_{con}(B)$ values and taken from Fig. 4. The parameters P_c, γ, and J_o as determined from the best theoretical fits to the experimental $J_c(B)$ data (see Figs. 5(a)–5(e)) for all the samples are listed in Table III (only the values at 5 and 25 K are shown). The P_c values of various *in-situ* samples are found to lie in a range 0.57 ± 0.04 and 0.59 ± 0.06 at 5 K and 25 K, respectively, which are higher than theoretically expected values ~0.2–0.3.[32] The observed higher values of P_c suggest that contribution of WLNs in the overall J_c of the samples cannot be ruled out. This conclusion is based on our discussion of *ex-situ* processed MgB_2 samples reported earlier,[29] where the observed values of $P_c = 0.70 \pm 0.05$ were much higher. On the other hand, the values of $\gamma = 4.9 \pm 0.5$ at 5 K and 3.9 ± 0.5 at 25 K in the *in-situ* samples are found to be higher than $\sim 3.9 \pm 1.2$ reported earlier[29] for the *ex-situ* samples. These results show that P_c and γ are sample dependent and contribute in the overall determination of $J_c(B)$.

Finally, in the light of above analysis, we underline the difference between our present *in-situ* and the earlier[29] reported *ex-situ* processed MgB_2 samples. *In-situ* processing led to significant improvement in connectivity, so that the $J_c(B,T)$ in terms of scaling behaviour and point core pinning mechanism became clearly visible. Whereas, in the case of *ex-situ* processing due to poorer connectivity, both pinning and WLNs compete in determining the overall $J_c(B,T)$. Interestingly, in both the cases: (a) excess Mg as an additive led to highest $J_c(B, T)$; and (b) addition of non-carbon additives along with excess Mg did not improve the J_c further, although it was higher in comparison to pure MB sample. We would like to mention that, though *in-situ* processing leads to a significant increase in low field J_c, the irreversibility fields B*(T) are lower in comparison to that of *ex-situ* processing. This indicates that *in-situ* processing could improve the $J_c(B)$ graph vertically, however, the horizontal improvement could not be achieved by mixing non-carbon based additives. The latter optimisation is very important for the high field applications and needs more effort especially for non-carbon based additives.

TABLE III. The values of $B_{c2}^{\parallel}(T)$, and the parameters P_c, γ, and J_0 (10^9 A/m^2) for various samples taken from the fits to Fig. 5.

	5 K				25 K			
	P_c	γ	J_o	$B_{c2}^{\parallel}$	P_c	γ	J_o	$B_{c2}^{\parallel}$
MB	0.57	4.4	4.9	18.84	0.65	3.4	1.1	7.34
MBMg	0.55	5.4	8.1	24.87	0.65	4.0	1.9	9.09
MBAg	0.58	4.8	5.0	21.30	0.60	3.8	1.2	7.80
MBNi	0.53	5.2	5.8	20.93	0.53	4.5	1.0	7.57
MBYB	0.62	5.4	6.4	21.57	0.66	4.3	1.5	7.83

V. CONCLUSION

In-situ processed bulk samples of pure MgB_2, with excess Mg (5 wt. %) and further 3 wt. % non-carbon based additives of nano-Ag, nano-Ni, and YBCO were investigated for structural, transport, and magnetic properties. The additives did not show any substitution in MgB_2 lattice and the superconducting transition stayed almost unaffected. The samples typically showed connectivity between 11%–20%. The magnetically determined irreversibility line of all the samples was found to lie much lower than the respective resistively determined $T_{con}(B)$ and $T_{c0}(B)$ lines in the B-T phase diagram. The $F_p(B, T)$ scaled perfectly in the entire B and T regions in all the samples and revealed a universal point core pinning mechanism. Both δl- and/or δT_c- type core pinning could be delineated in the samples. Based on anisotropy driven percolation model, it was shown that the parameters γ, P_c, and $B_{c2}^{\parallel}$ need to be taken into account for a quantitative comparison of $J_c(B, T)$ of different samples. To realize the true potential of the non-carbon additives acting as pinning centres in optimized MgB_2 host sample needs more work.

ACKNOWLEDGMENTS

We gratefully acknowledge the help of Dr. R. Rawat (UDCSR, Indore) for high field resistivity and Dr. H. Huhtinen (WPL, University of Turku, Finland) for high field magnetization measurements. The experimental facilities used at UDCSR were provided by DST and UGC. The authors (from NPL) thank Director NPL for his encouragement. H.K. thanks CSIR, New Delhi for the financial support through Emeritus Scheme. A.V.N. thanks INSA, New Delhi for financial support.

[1]J. Nagamatsu, N. Nakagawa, T. Muranaka, Y. Zenitani, and J. Akimitsu, Nature **410**, 63 (2001).
[2]Z. X. Shi, A. K. Pradhan, M. Tokunaga, K. Yamazaki, T. Tamegai, Y. Takano, K. Togano, H. Kito, and H. Ihara, Phys. Rev. B **68**, 104514 (2003).
[3]J. H. Kim, S. X. Dou, M. S. A. Hossain, X. Xu, J. L. Wang, D. Q. Shi, T. Nakane, and H. Kumakura, Supercond. Sci. Technol. **20**, 715 (2007).
[4]C. Wang, Y. Ma, X. Zhang, D. Wang, Z. Gao, C. Yao, C. Wang, H. Oguro, S. Awaji, and K. Watanabe, Supercond. Sci. Technol. **25**, 035018 (2012).
[5]H. Tanaka, A. Yamamoto, Jun -ichi Shimoyama, H. Ogino, and K. Kishio, Supercond. Sci. Technol. **25**, 115022 (2012).
[6]A. Kario, R. Nast, W. Habler, C. Rodig, C. Mickel, W. Goldacker, B. Holzapfel, and L. Schultz, Supercond. Sci. Technol. **24**, 075011 (2011).
[7]A. Kario, W. Häbler, C. Rodig, M. Schubert, P. Kovác, T. Melišek, R. Nast, W. Goldacker, and B. Holzapfel, J. Supercond. Novel Magn. **25**, 2337 (2012).
[8]H. Yamada, N. Uchiyama, A. Matsumoto, H. Kitaguchi, and H. Kumakura, Supercond. Sci. Technol. **20**, 1 (2007).
[9]D. Wang, C. Wang, X. Zhang, Z. Gao, C. Yao, Y. Ma, M. Kanazawa, Y. Yamada, H. Oguro, S. Awaji, and K. Watanabe, Supercond. Sci. Technol. **25**, 065013 (2012).
[10]S. X. Dou, S. Soltanian, J. Horvat, X. L. Wang, S. H. Zhou, M. Ionescu, H. K. Liu, P. Munroe, and M. Tomsic, Appl. Phys. Lett. **81**, 3419 (2002).

[11]M. J. Qin, X. L. Wang, H. K. Liu, and S. X. Dou, Phys. Rev. B **65**, 132508 (2002).
[12]S. L. Prischepa, M. L. D. Rocca, L. Maritato, M. Salvato, R. D. Capua, M. G. Maglione, and R. Vaglio, Phys. Rev. B **67**, 024512 (2003).
[13]I. Pallecchi, C. Tarantini, H. U. Aebersold, V. Braccini, C. Fanciulli, C. Ferdeghini, F. Gatti, E. Lehmann, P. Manfrinetti, D. Marré, A. Palenzona, A. S. Siri, M. Vignolo, and M. Putti, Phys. Rev. B **71**, 212507 (2005).
[14]K. S. Tan, S. K. Chen, B.-H. Jun, and C.-J. Kim, Supercond. Sci. Technol. **21**, 105013 (2008).
[15]Z. X. Shi, M. A. Susner, M. D. Sumption, E. W. Collings, X. Peng, M. Rindfleisch, and M. J. Tomsic, Supercond. Sci. Technol. **24**, 065015 (2011).
[16]H. Fujii, K. Ozawa, and H. Kitaguchi, Supercond. Sci. Technol. **25**, 065008 (2012).
[17]W. K. Yeoh and S. X. Dou, Physica C **456**, 170 (2007).
[18]S. X. Dou, O. Shcherbakova, W. K. Yeoh, J. H. Kim, S. Soltanian, X. L. Wang, C. Senatore, R. Flukiger, M. Dhalle, O. Husnjak, and E. Babic, Phys. Rev. Lett. **98**, 097002 (2007).
[19]S. X. Dou, S. Soltanian, Y. Zhao, E. Getin, Z. Chen, O. Shcherbakova, and J. Horvat, Supercond. Sci. Technol. **18**, 710 (2005).
[20]C. S. Lue, T. H. Su, B. X. Xie, S. K. Chen, J. L. MacManus-Driscoll, Y. K. Kuo, and H. D. Yang, Phys. Rev. B **73**, 214505 (2006).
[21]Q. Zhao, Y. Liu, S. Penner, L. Yu, Z. Dong, and Z. Gao, Supercond. Sci. Technol. **22**, 075024 (2009).
[22]Q. Cai, Z. Ma, Q. Zhao, and Y. Liu, J. Supercond. Novel Magn. **24**, 2013 (2011).
[23]D. Kumar, S. J. Pennycook, J. Narayan, H. Wang, and A. Tiwari, Supercond. Sci. Technol. **16**, 455 (2003).
[24]C. Shekhar, R. Giri, R. S. Tiwari, O. N. Srivastava, and S. K. Malik, J. Appl. Phys. **101**, 043906 (2007).
[25]E. Kuzmann, Z. Homonnay, Z. Klencsar, M. Kuhberger, A. Vertes, and G. Gritzner, Supercond. Sci. Technol. **15**, 1479 (2002).
[26]X. F. Rui, X. F. Sun, X. L. Xu, L. Zhang, and H. Zhang, Int. J. Mod. Phys. B **19**, 375 (2005).
[27]R. Zeng, L. Lu, J. L. Wang, J. Horvat, W. X. Li, D. Q. Shi, S. X. Dou, M. Tomsic, and M. Rindfleisch, Supercond. Sci. Technol. **20**, L43 (2007).
[28]A. Gupta, A. Kumar, and A. V. Narlikar, Supercond. Sci. Technol. **22**, 105005 (2009).
[29]P. P. S. Bhadauria, A. Gupta, H. Kishan, and A. V. Narlikar, J. Appl. Phys. **113**, 063908 (2013).
[30]J. M. Rowell, Supercond. Sci. Technol. **16**, R17 (2003).
[31]G. Blatter, M. Y. Feigel'man, Y. B. Geshkenbein, A. I. Larkin, and V. M. Vinokur, Rev. Mod. Phys. **66**, 1125 (1994).
[32]M. Eisterer, M. Zehetmayer, and H. W. Weber, Phys. Rev. Lett. **90**, 247002 (2003).
[33]P. Lezza, R. Gladyshevskii, H. L. Suo, and R. Flukiger, Supercond. Sci. Technol. **18**, 753 (2005).
[34]A. Gupta and A. V. Narlikar, Supercond. Sci. Technol. **22**, 125029 (2009).
[35]D. D. Hughes, Philos. Mag. **30**, 293 (1974).
[36]R. Griessen, W. Hai-hu, A. J. J. van Dalen, B. Dam, J. Rector, and H. G. Schnack, Phys. Rev. Lett. **72**, 1910 (1994).